Resonance-enhanced optical forces between coupled photonic crystal slabs

**Victor Liu,[1] Michelle Povinelli,[2]
and Shanhui Fan[1,*]**

[1]*Department of Electrical Engineering, Stanford University, Stanford, California 94305*
[2]*Ming Hsieh Department of Electrical Engineering, University of Southern California, Los Angeles, California 90089*
*shanhui@stanford.edu

Abstract: The behaviors of lateral and normal optical forces between coupled photonic crystal slabs are analyzed. We show that the optical force is periodic with displacement, resulting in stable and unstable equilibrium positions. Moreover, the forces are strongly enhanced by guided resonances of the coupled slabs. Such enhancement is particularly prominent near dark states of the system, and the enhancement effect is strongly dependent on the types of guided resonances involved. These structures lead to enhancement of light-induced pressure over larger areas, in a configuration that is directly accessible to externally incident, free-space optical beams.

References and links

1. M. L. Povinelli, M. Ibanescu, S. Johnson, and J. D. Joannopoulos, "Slow-light enhancement of radiation pressure in an omnidirectional-reflector waveguide," Appl. Phys. Lett. **85**(9), 1466–1468 (2004), http://link.aip.org/link/?APL/85/1466/1.
2. M. L. Povinelli, M. Lončar, M. Ibanescu, E. J. Smythe, S. G. Johnson, F. Capasso, and J. D. Joannopoulos, "Evanescent-wave bonding between optical waveguides," Opt. Lett. **30**(22), 3042–3044 (2005), http://ol.osa.org/abstract.cfm?URI=ol-30-22-3042.
3. M. L. Povinelli, S. G. Johnson, M. Lončar, M. Ibanescu, E. J. Smythe, F. Capasso, and J. D. Joannopoulos, "High-Q enhancement of attractive and repulsive optical forces between coupled whispering-gallery-mode resonators," Opt. Express **13**(20), 8286–8295 (2005), http://www.opticsexpress.org/abstract.cfm?URI=oe-13-20-8286.
4. A. Mizrahi, and L. Schächter, "Two-slab all-optical spring," Opt. Lett. **32**(6), 692–694 (2007), http://ol.osa.org/abstract.cfm?URI=ol-32-6-692.
5. M. Eichenfield, C. P. Michael, R. Perahia, and O. Painter, "Actuation of Micro-Optomechanical Systems Via Cavity-Enhanced Optical Dipole Forces," Nat. Photon. **1**, 416–422 (2007), *http://dx.doi.org/10.1038/nphoton.2007.96*.
6. J. Ng, and C. T. Chan, "Size-selective optical forces for microspheres using evanescent wave excitation of whispering gallery modes," Appl. Phys. Lett. **92**(25), 251109 (2008), http://link.aip.org/link/?APL/92/251109/1.
7. M. Li, W. H. Pernice, C. Xiong, T. Baehr-Jones, M. Hochberg, and H. X. Tang, "Harnessing optical forces in integrated photonic circuits," Nature **456**(7221), 480–484 (2008), http://dx.doi.org/10.1038/nature07545.
8. H. Taniyama, M. Notomi, E. Kuramochi, T. Yamamoto, Y. Yoshikawa, Y. Torii, and T. Kuga, "Strong radiation force induced in two-dimensional photonic crystal slab cavities," Phys. Rev. B **78**(16), 165129 (2008), http://link.aps.org/doi/10.1103/PhysRevB.78.165129.
9. W. H. P. Pernice, M. Li, and H. X. Tang, "Theoretical investigation of the transverse optical force between a silicon nanowire waveguide and a substrate," Opt. Express **17**(3), 1806–1816 (2009), http://www.opticsinfobase.org/abstract.cfm?URI=oe-17-3-1806.
10. M. Eichenfield, J. Chan, R. Camacho, K. J. Vahala, and O. Painter, "Optomechanical Crystals," *http://arxiv.org/abs/0906.1236*.
11. G. S. Wiederhecker, L. Chen, A. Gondarenko, and M. Lipson, "Controlling photonic structures using optical forces", *http://arxiv.org/abs/0904.0794*.
12. V. N. Astratov, J. S. Culshaw, R. M. Stevenson, D. M. Whittaker, M. S. Skolnick, T. F. Krauss, and R. M. de la Rue, "Resonant coupling of near-infrared radiation to photonic band structure waveguides," J. Lightwave Technol. **17**(11), 2050–2057 (1999).
13. S. Fan, and J. D. Joannopoulos, "Analysis of guided resonances in photonic crystal slabs," Phys. Rev. B **65**(23), 235112 (2002), http://link.aps.org/doi/10.1103/PhysRevB.65.235112.
14. T. Ochiai, and K. Sakoda, "Dispersion relation and optical transmittance of a hexagonal photonic crystal slab," Phys. Rev. B **63**(12), 125107 (2001), http://link.aps.org/doi/10.1103/PhysRevB.63.125107.

15. W. Suh, M. F. Yanik, O. Solgaard, and S. Fan, "Displacement-sensitive photonic crystal structures based on guided resonance in photonic crystal slabs," Appl. Phys. Lett. **82**(13), 1999–2001 (2003), http://link.aip.org/link/?APL/82/1999/1.
16. V. R. Almeida, Q. Xu, C. A. Barrios, and M. Lipson, "Guiding and confining light in void nanostructure," Opt. Lett. **29**(11), 1209–1211 (2004), http://www.opticsinfobase.org/ol/abstract.cfm?URI=ol-29-11-1209.
17. D. M. Whittaker, and I. S. Culshaw, "Scattering-matrix treatment of patterned multilayer photonic structures," Phys. Rev. B **60**(4), 2610–2618 (1999), http://link.aps.org/doi/10.1103/PhysRevB.60.2610.
18. M. Liscidini, D. Gerace, L. C. Andreani, and J. E. Sipe, "Scattering-matrix analysis of periodically patterned multilayers with asymmetric unit cells and birefringent media," Phys. Rev. B **77**(3), 035324 (2008), http://link.aps.org/doi/10.1103/PhysRevB.77.035324.
19. M. I. Antonoyiannakis, and J. B. Pendry, "Electromagnetic forces in photonic crystals," Phys. Rev. B **60**(4), 2363–2374 (1999), http://link.aps.org/doi/10.1103/PhysRevB.60.2363.
20. J. D. Jackson, *Classical Electrodynamics*, (Wiley, New York, 1998).
21. S. Fan, W. Suh, and J. D. Joannopoulos, "Temporal coupled-mode theory for the Fano resonance in optical resonators," J. Opt. Soc. Am. A **20**(3), 569–572 (2003), http://www.opticsinfobase.org/josaa/abstract.cfm?URI=josaa-20-3-569.
22. S. G. Johnson, and J. D. Joannopoulos, "Block-iterative frequency-domain methods for Maxwell's equations in a planewave basis," Opt. Express **8**(3), 173–190 (2001), http://www.opticsexpress.org/abstract.cfm?URI=OPEX-8-3-173.
23. W. Suh, O. Solgaard, and S. Fan, "Displacement sensing using evanescent tunneling between guided resonances in photonic crystal slabs," J. Appl. Phys. **98**(3), 033102 (2005), http://link.aip.org/link/?JAPIAU/98/033102/1.
24. S. E. Harris, "Electromagnetically induced transparency," Phys. Today **50**(7), 36–42 (1997).
25. Q. Xu, S. Sandhu, M. L. Povinelli, J. Shakya, S. Fan, and M. Lipson, "Experimental realization of an on-chip all-optical analogue to electromagnetically induced transparency," Phys. Rev. Lett. **96**(12), 123901 (2006), http://link.aps.org/abstract/PRL/v96/e123901.
26. M. Barth, and O. Benson, "Manipulation of dielectric particles using photonic crystal cavities," Appl. Phys. Lett. **89**(25), 253114 (2006), http://link.aip.org/link/?APPLAB/89/253114/1.

1. Introduction

There has been significant interest in using optical forces for applications such as manipulating nanoscale systems, optical cooling of mechanical motion of mesoscopic objects, and demonstrating novel nonlinear optical effects [1–11]. The systems studied so far include coupled waveguides, waveguides coupled to substrates, as well as a variety of resonator structures such as micro-rings, disks or toroids that support whispering gallery modes, and point defects in photonic crystal slab structures that support standing-wave optical modes.

In this paper we study optical forces between coupled photonic crystal slabs, in an exemplary system as shown in Fig. 1. We find that, due to in-plane periodicity of the structure, lateral and normal forces exhibit periodic dependence on position, leading to unstable and stable equilibrium positions. Moreover, near the frequencies of guided resonances, we see significant enhancement of the optical forces. In these systems, the presence of in-plane periodic index contrast enables phase-matched coupling between externally incident planewaves and guided modes that are supported by the slab, leading to strong resonant behaviors of individual slabs [12, 13]. The interaction between these resonances in two slabs (Fig. 1) leads to a rich set of effects and opportunities for optical force enhancement. In comparison to previous works, these structures lead to enhancement of light-induced pressure over larger areas, in a configuration that is directly accessible to externally incident, free-space optical beams.

One of the most intriguing aspects of guided resonances in photonic crystal slabs is the existence of dark states. These are states with their frequency and in-plane wavevectors satisfying the phase-matching conditions for coupling to external plane waves, and are nevertheless de-coupled from external planewaves due to either symmetric or dynamic reasons [14, 15]. Here we show that in spite of the fact that light cannot directly couple to these states, their presence nevertheless leads to divergence of light-induced pressure as a function of the displacement. Moreover, the characteristics of the divergence are intimately related to the nature of the dark states.

The paper is organized as follows. In Section 2 we discuss the model system of a photonic crystal slab and the scattering matrix method used to compute the fields and forces. Section 3 provides an overview of the modal properties and transmission behaviors of photonic crystal slab systems. Section 4 describes the behavior of optical forces as a function of the slab

position. Section 5 discusses the behavior and divergence of optical forces under various displacements. Finally, Section 6 provides estimates of the magnitude of forces in practically realizable systems.
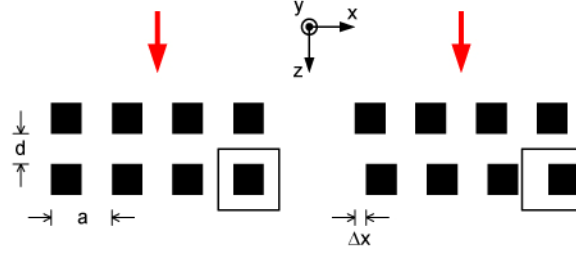

Fig. 1. Schematic of the double slab system. The red arrows indicate the directions of the incident light. Each slab consists of an array of high index rods ($\varepsilon = 12$) surrounded by air ($\varepsilon = 1$). The empty rectangle indicates the surface over which the integration of the stress tensor is performed. In the right panel, the bottom slab is shifted relative to the first slab by a distance Δx.

2. Model system and computational methods

We focus on systems consisting of two periodically patterned dielectric slabs (Fig. 1). Each slab consists of equally sized alternating regions of high-index material ($\varepsilon = 12$ is used throughout this work) and air ($\varepsilon = 1$), with lattice constant a. The thickness of each slab is $0.5a$. The two slabs are separated from each other by an edge-to-edge distance d. Moreover the two slabs are possibly laterally shifted by Δx along the x-direction. The excitation is assumed to be a normally incident planewave with electric field in the y-direction. The effects described here are quite general and apply to the alternate incident wave polarization as well. However, in the case of an electric field polarized in the x-direction, there is the possibility of field concentration in the air regions [16], which could possibly provide additional force [16]. We here use a field in the y-direction to explicitly focus on the resonance effect.

Throughout this work we use the scattering matrix method (SMM) to compute both the transmission through the slabs and their optical force properties [17, 18]. In this technique, the simulated structures are divided into layers along the z-direction. Each layer is uniform along the z-direction.

As a first step, one determines the eigenmodes that are appropriate for each layer, by considering a corresponding infinite structure that has the same dielectric profile in the xy-plane, but is uniform and infinite in the z-direction. For such a corresponding infinite structure, the electric field distribution of its eigenmodes has the form:

$$\mathbf{u}_{n,m}(\mathbf{r},z) = \sum_{\mathbf{G}} \mathbf{u}_{n,m}(\mathbf{G}) \exp\left[i(\mathbf{k}+\mathbf{G})\cdot\mathbf{r}\right] \exp\left[iq_{n,m}z\right] \tag{1}$$

Here $\mathbf{r} = (x,y)$. $\mathbf{k} = (k_x, k_y)$ is the in-plane wavevector for the incident wave. The summation is over all reciprocal lattice vectors $\mathbf{G}$'s. The subscripts n and m label the m-th mode for the n-th layer. Both $u_{n,m}(\mathbf{G})$ and the square of the longitudinal wavevectors, i.e. $q_{n,m}^2$, correspond to the m-th eigenmode and eigenvalue of an $N_{\mathbf{G}} \times N_{\mathbf{G}}$ matrix, obtained by expressing Maxwell's equations in the planewave basis. $N_{\mathbf{G}}$ is the number of planewaves used. Notice that in general $q_{n,m}$ can be complex.

Using the eigenmodes as a basis, the field in the n-th layer can then be expanded as

$$\mathbf{E}_n(\mathbf{G},z) = \sum_m \mathbf{u}_{n,m}(\mathbf{G}) \left[a_{n,m} \exp\left(iq_{n,m}z\right) + b_{n,m} \exp\left(-iq_{n,m}z\right) \right] \tag{2}$$

Here the forward and backward wave mode amplitudes are $a_{n,m}$ and $b_{n,m}$, respectively.

Suppose a planewave is incident upon the structure from the air region above. In the air region above, we set all incoming planewave amplitudes to zero except for the actual incident wave. By matching boundary conditions at all interfaces, a linear system can be set up to determine all the *a* and *b* coefficients [17], and thus obtaining the field in the entire structure. This procedure provides exact results for a dielectric function of a finite number of Fourier components. But the results below, which use 27 plane-wave components to approximate a square wave dielectric profile, achieve good convergence (within 0.1% in the force computations).

The force on the structure is evaluated using the Maxwell stress tensor formalism [19, 20]. The time-averaged force on a rigid dielectric body can be found by an integral over an oriented surface completely enclosing the object:

$$\langle F_\alpha \rangle = \int \langle T_{\alpha\beta} \rangle dS_\beta \qquad (3)$$

where the subscripts α and β each vary over (x, y, z), and repeated indices are summed over all possible values. Here dS_β is the area element with outward normal vector. The time-averaged stress tensor $\langle T_{\alpha\beta} \rangle$ is defined as

$$\langle T_{\alpha\beta} \rangle = \frac{1}{2}\Re\left[E_\alpha D_\beta^* + H_\alpha B_\beta^* - \frac{1}{2}\delta_{\alpha\beta}\left(E_\gamma D_\gamma^* + H_\gamma B_\gamma^* \right) \right] \qquad (4)$$

We choose to integrate this tensor over a rectangular box enclosing the unit cell of one of the slabs. Contributions to the stress tensor from the sides parallel to the *z*-axis cancel due to the opposite orientation of the normal vectors for the two sides and the Bloch periodicity of the fields. Therefore, the integral only needs to be evaluated on the two surfaces normal to the *z*-direction on either side of a slab.

Combining Eqs. (1) and (2) we see that at any plane perpendicular to the *z*-axis, the fields can be expressed in a planewave expansion over a set of reciprocal lattice vectors **G** :

$$\mathbf{E}(z) = \sum_{\mathbf{G}} \mathbf{e}(\mathbf{G}) \exp\left[i(k+\mathbf{G})\cdot\mathbf{r} \right] \qquad (5)$$

where $\mathbf{e}(\mathbf{G})$ is *z*-dependent. Substituting this form into Eq. (4) greatly simplifies the computation. For example, the first term is simply

$$\frac{1}{2}\Re\int E_\alpha D_z^* dS_z = \frac{1}{2}\Re\int \sum_{\mathbf{G}}\sum_{\mathbf{G}'} e_\alpha(\mathbf{G}) d_z^*(\mathbf{G}') \exp[i\mathbf{G}\cdot\mathbf{r}]\exp[-i\mathbf{G}'\cdot\mathbf{r}] dS_z$$
$$= \frac{A}{2}\Re\sum_{\mathbf{G}} e_\alpha(\mathbf{G}) d_z^*(\mathbf{G}) \qquad (6)$$

where *A* is the area of the unit cell, e_α is the α-component of $\mathbf{e}(\mathbf{G})$, and the other subscripted lowercase italic variables are the components of the corresponding fields expanded analogous to Eq. (5). Similarly, the total time-averaged force can be found by summing the contributions from the two surfaces, each of which has the form

$$\frac{A}{2}\Re\sum_{\mathbf{G}}\left[e_\alpha(\mathbf{G}) d_z^*(\mathbf{G}) + h_\alpha(\mathbf{G}) b_z^*(\mathbf{G}) - \frac{1}{2}\delta_{\alpha z}\left(e_\gamma(\mathbf{G}) d_\gamma^*(\mathbf{G}) + h_\gamma(\mathbf{G}) b_\gamma^*(\mathbf{G}) \right) \right] \quad (7)$$

Therefore, the force can be found efficiently once the Fourier coefficients have been obtained. Since in the SMM the fields are always expressed in terms of Fourier coefficients, this formalism is particularly well suited to the SMM.

3. General behaviors of the lateral and normal forces

We first comment on some of the general aspects of forces in this structure. These aspects, since they arise from the symmetry of the structure, apply both to the force at a constant incident power, as well as the force at a constant energy inside the structure, i.e. force per photon inside the structure. The structure is periodic in the x-direction. Also, a relative shift Δx of the two slabs by a distance a along the x-direction results in the same structure. It follows then that both the lateral force F_x and the normal force F_z are periodic with respect to the relative shift of the slabs, i.e.

$$F_x(\Delta x) = F_x(\Delta x + a)$$
$$F_z(\Delta x) = F_z(\Delta x + a)$$

(8)

In addition, the structure has a mirror plane symmetry perpendicular to the x-direction for both $\Delta x = 0$ and $\Delta x = 0.5a$. Thus, the normal force satisfies the additional constraints:

$$F_z(\Delta x) = F_z(-\Delta x)$$
$$F_z(\Delta x) = F_z(a - \Delta x)$$

(9)

which imply that the normal force F_z reaches an extremum at these two symmetric configurations. The same mirror symmetry also requires that the lateral force F_x satisfy

$$F_x(\Delta x) = -F_x(-\Delta x)$$
$$F_x(\Delta x) = -F_x(a - \Delta x)$$

(10)

As a result, the lateral force vanishes at the two symmetric configurations with $\Delta x = 0$ and $\Delta x = 0.5a$. If the two slabs are constrained to move in only the x direction, these two symmetric configurations represent equilibrium situations. They can be either stable or unstable. In the case as shown in Fig. 2(a), for example, $\Delta x = 0$ is stable while $\Delta x = 0.5a$ is unstable.
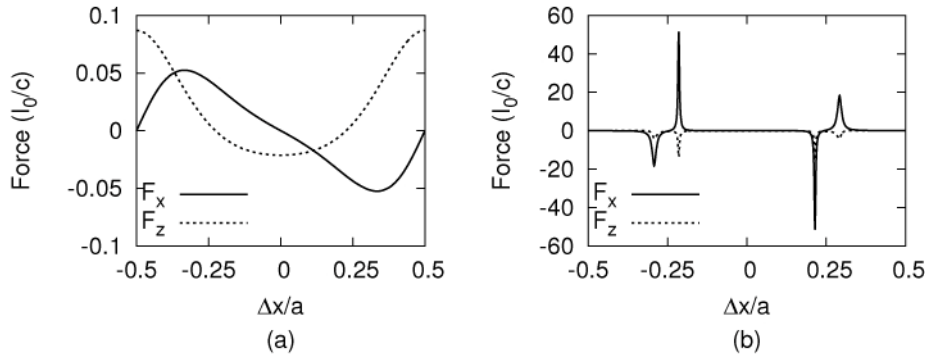

Fig. 2. Lateral and normal forces as functions of relative shift in the horizontal direction between the slabs. The vertical spacing between the slabs is $d = 0.5a$. The forces are periodic with respect to the displacement. Only one period in Δx is shown. (a) Far from resonance at $\omega = 0.57 \times 2\pi c / a$. (b) Near resonance at $\omega = 0.58 \times 2\pi c / a$. Note the vastly different vertical scales.

The conditions (8)-(10) above arise from general symmetry properties of the slab, and thus are satisfied at all operating frequencies, as can be seen in Fig. 2. The detailed behavior of the optical forces, however, is strongly influenced by the modal properties of the system and is therefore drastically different as frequency varies. In Fig. 2(a), the force variation as a function of relative shift Δx is plotted at a frequency of $\omega = 0.57 \times 2\pi c / a$, far from any

resonance. The force is given in units proportional to the incident power flux I_0. The forces vary smoothly with respect to the relative shift between the slabs. In Fig. 2(b), the forces are plotted at $\omega = 0.58 \times 2\pi c / a$, which happens to be near a resonance of the two-slab system with a relative shift of $\Delta x = 0.2a$. The forces are greatly enhanced when the relative shift between the slabs creates a resonance at the operating frequency. In the following sections, we will provide a detailed analysis of the resonant enhancement of optical forces in this system.

4. Modal properties of single and double photonic crystal slabs

The nature of the optical force between the slabs is intimately related to the nature of guided resonances in the coupled slab system, which in turn, can be understood by studying the resonances in the single slab case.

A single slab possesses guided resonances, which are modes that are strongly confined by the slab, but nevertheless can couple to external radiation and therefore in principle have a finite lifetime. The presence of a guided resonance in a photonic crystal slab is manifested as a Fano line shape in the transmission spectrum superimposed on an otherwise smooth background [21], as shown in Fig. 3(a). Both the frequency and the modal profile of the guided resonance can be obtained using a separate photonic band structure code (MPB) [22]. The transmission spectrum always goes through a perfect zero and unity in the vicinity of the guided resonance frequency. The modal profile of such guided resonance is shown in the top panel of Fig. 3(b). The bottom panel of the same figure shows the mode being excited by an external planewave source. We will refer to such a guided resonance as a "bright guided resonance."

In addition to the bright guided resonance, the single slab system also possesses "dark guided resonances" that cannot be seen in the transmission spectrum. These modes exist above the light line and hence would have been able to couple to radiation modes from band folding arguments alone. However they possess multipole-like mode-field distributions that, due to symmetry, have a vanishing overlap integral with the incident radiation modes. These modes do not couple to external radiation, and are therefore dark states [13, 14]. As an example, in the simulations, mode-solving reveals the presence of a mode with a quadrupole-like field distribution inside the rod at a frequency of $0.58 \times 2\pi c / a$, (Fig. 4(b), top panel). In contrast, the transmission spectrum does not have any sharp spectral features at the mode frequency (Fig. 4(a).). Instead, at the mode frequency an incident planewave passes through the slab without exciting the mode, as shown in the bottom panel of Fig. 4(b). A dark state like this possesses an infinite quality-factor (or Q-factor).

Based on the discussions above on guided resonances in single slabs, we now consider dark states in two-slab systems. Here, as we will show below, there are actually two different mechanisms to create dark states, arising from the interaction of either bright or dark guided resonances in the single slab. In the first mechanism, the dark state occurs at the condition where the spacing between the two slabs takes specific values. In the second mechanism, the dark state occurs at the condition where the two slabs are arranged in a configuration such that the overall structure has a mirror symmetry. Small deviations from either of these conditions lead to states with very high quality factors, and moreover with such quality factors strongly dependent upon mechanical displacements. (We will refer to such states that are linked to the dark states as "near-dark states" below.) As a result, the presence of dark states in two-slab systems has important implications for the optical force between them.

4.1 Dark state arising from coupled bright resonances

In the single slab system, near a bright guided resonance there always exists a frequency for which total reflection occurs. Therefore, one can form a dark state in the two-slab system, by choosing an appropriate spacing (referred to as d_∞ below) between the slabs, such that a Fabry-Perot resonance between the two slabs is formed exactly at the frequency where the

reflectivity of each individual slab reaches unity [23]. In the system shown in Fig. 3, $d_\infty = 0.65a$, at the slab spacing $d = d_\infty$, the state is decoupled from external radiation.
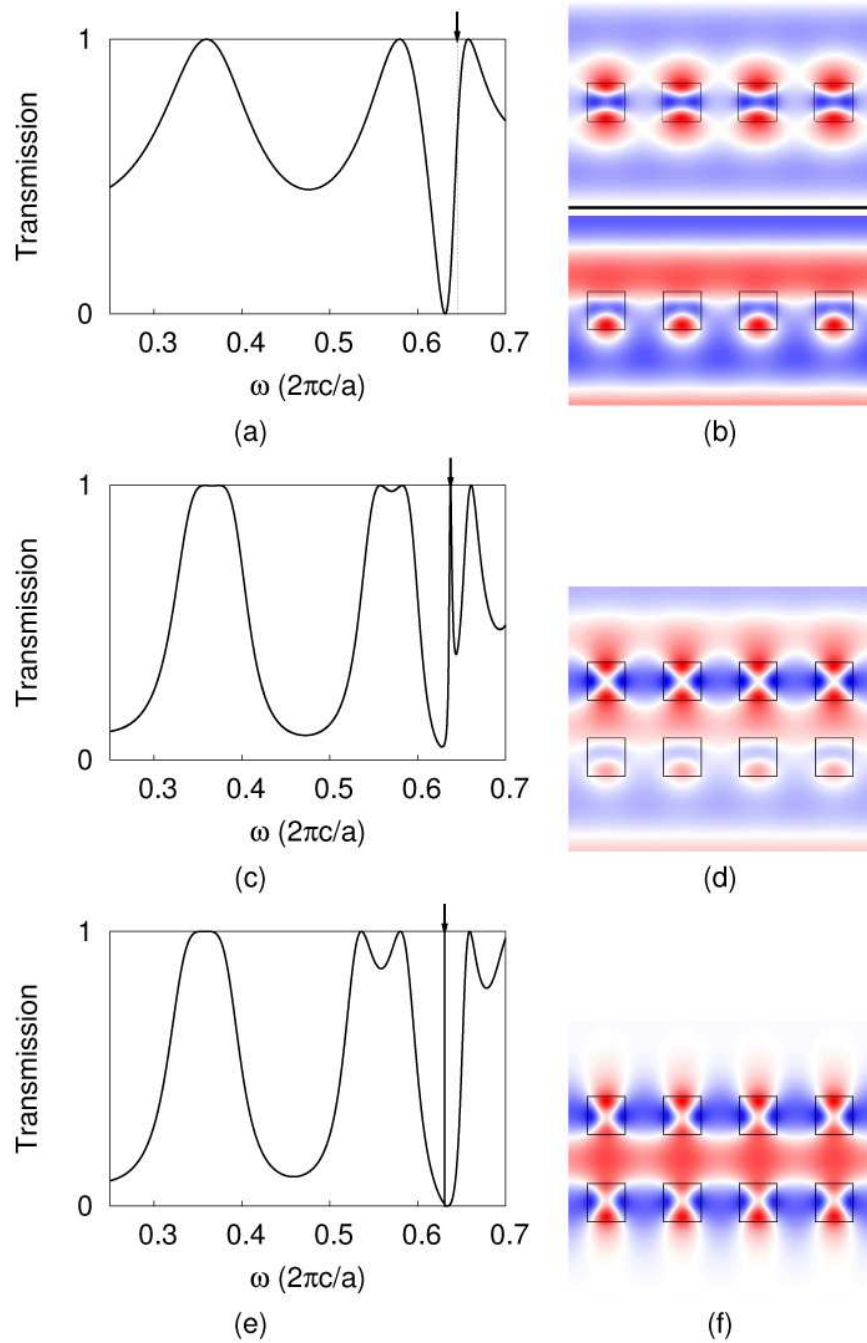

Fig. 3. Dark state arising from coupled bright guided resonances: (a) Single slab transmission spectrum; the arrow indicates the frequency of a Fano resonance mode. (b) Mode profile calculated by MPB (top) and field profile computed with SMM at the frequency indicated by the arrow in (a) (bottom). (c) Double slab transmission spectrum for $d = 0.5a$. (d) Field profile at frequency indicated by the arrow in (c). (e) Double slab transmission spectrum for $d = 0.65a$; note the extremely sharp resonance peak. (f) Field profile at peak of resonance in (e).

When the slab spacing d is in the vicinity of d_∞ (Figs. 3(c) and 3(e)), the transmission spectrum of the system exhibits a lineshape that is analogous to the Electromagnetically Induced Transparency (EIT) effect in atomic systems [24], where a sharp transparency resonance peak exists within the center of a broad resonance dip [15, 25]. Moreover, in comparing Fig. 3(c) ($d = 0.5a$), with Fig. 3(e) ($d = 0.65a$), we see that the width of the transmission peak becomes narrower, and in fact the quality factor of the transparency resonance peak diverges as d approaches d_∞. Corresponding to Figs. 3(c) and 3(e), the steady state field distributions at the frequencies of the resonance peak are shown in Figs. 3(d) and 3(f), respectively. The higher-Q state in Fig. 3(f) exhibits a much weaker coupling to the external radiation. To summarize, one can start with a bright resonance in a single photonic crystal slab and introduce a second slab to create a near-dark state with a much higher quality factor. The quality factor is mechanically tunable over a wide range by adjusting the slab spacing.

4.2 Dark state arising from coupled dark resonances

In the single slab system, as indicated above, there exist dark guided resonances that are uncoupled to external radiation due to the mirror symmetry of the structure. In the system of two slabs, the two dark modes from the two slabs couple to one another to form two coupled modes. However, if the two slabs are vertically aligned ($\Delta x = 0$), the system remains symmetric, and thus both of these coupled modes are dark and do not couple to external radiation. The transmission spectrum of the symmetric two-slab system is shown in Fig. 4(c). There is indeed no spectral signature in the vicinity of the dark resonances.

By laterally shifting the two slabs relative to one other, the mirror symmetry of the system is broken [15]. As a result, the two coupled modes above can couple to external radiation, resulting in two Fano lineshapes in close proximity to each other (Fig. 4(e)). Such a Fano lineshape arises from the interference of the incident radiation with the guided resonance. Comparing the field distributions of the unshifted (Fig. 4(d)) and the shifted systems (Fig. 4(f)), we note that the shift of the slabs allows the excitation of a state with a very different local modal profile. In summary, one can start with a dark resonance in a single photonic crystal slab and introduce a second slab to create a near-dark state, with a quality factor that is highly sensitive to the horizontal displacement between the slabs.

5. Optical forces

In general, it is known that the optical force can be drastically enhanced with the use of high-Q resonances. The dark states for the two-slab systems are infinite-Q states that exist at specific frequencies and at specific displacements between the two slabs. In the vicinity of these special frequencies and displacements, the system exhibits high-Q near-dark states, which results in enhanced optical forces.

Corresponding to the two cases of dark states in the two slab system, below we will consider three different scenarios to reveal some of the relevant physics of force enhancement in the vicinity of these dark states. In Cases 1 and 3, we will consider the behaviors of optical forces as a function of slab spacing, with the two slabs maintained in configurations that either possess, or break mirror symmetry, respectively. We will choose to operate in a frequency range close to the dark state discussed in Section 4.1, since the quality factor of such states strongly depends on the variation of the slab spacing. In Case 2, we will consider the behaviors of the forces as a function of relative shift between the slabs, with the two slabs maintained at a constant spacing. We will choose to operate in a frequency range close to the dark states as discussed in Section 4.2, since the quality factor of such states is strongly influenced by the relative shift between the slabs.
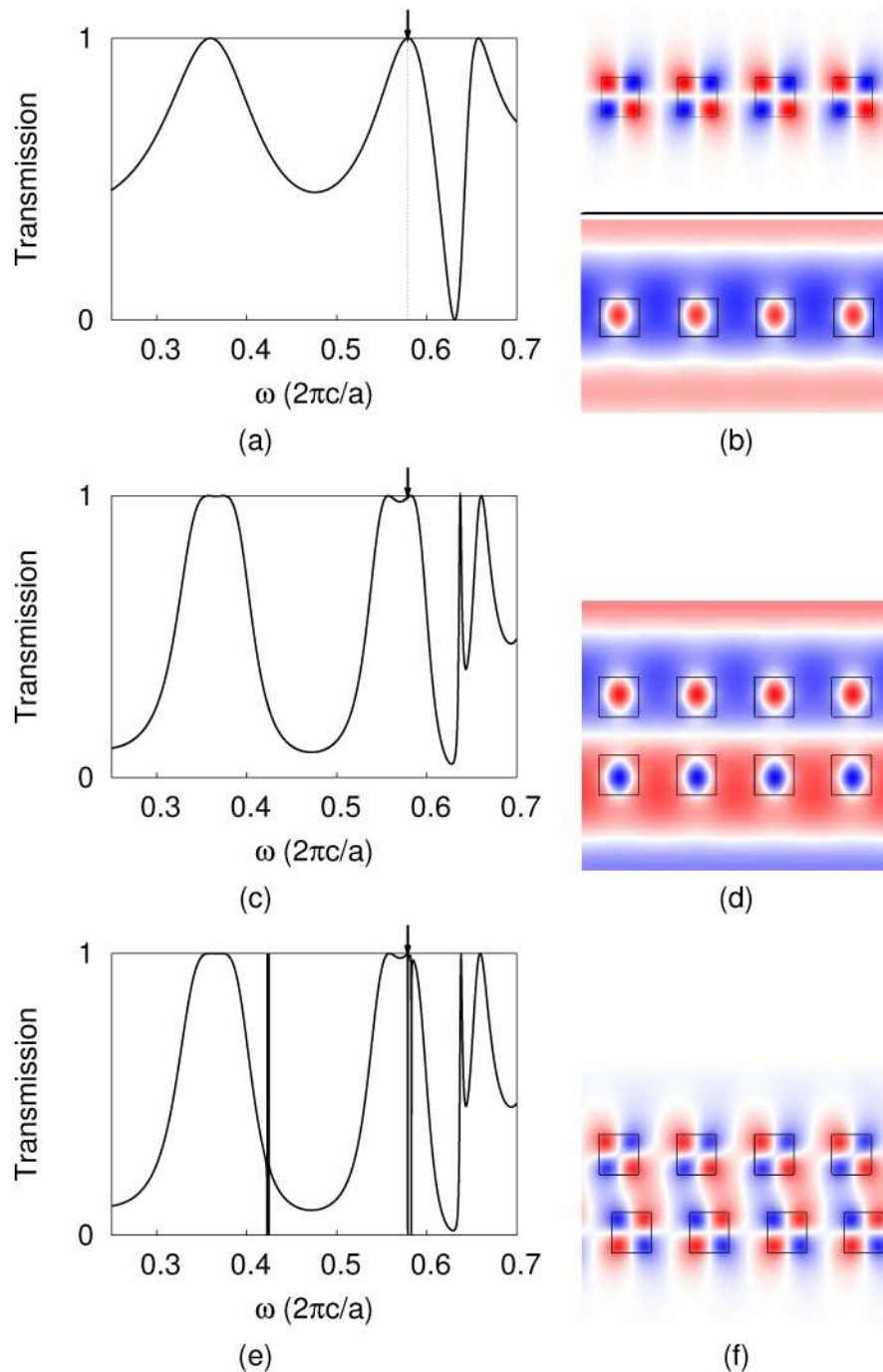
Fig. 4. Dark states in the two-slab system that arise from coupled dark resonances from single slabs: (a) Single slab transmission spectrum; the arrow indicates the frequency of a dark state. (b) Mode profile calculated from MPB at the dark state frequency (top) and field profile computed with SMM at the frequency indicated by the arrow in (a) (bottom). (c) Double slab transmission spectrum for $d = 0.5a$. (d) Field profile at frequency indicated by the arrow in (a). (e) Double slab transmission spectrum for $\Delta x = 0.15a$; note the appearance of pairs of sharp resonances. (f) Field profile at lowest frequency resonance from (e).

5.1 Case 1: Changing slab separation, symmetric case

We start by consider the configuration corresponding to Figs. 3(d) and 3(e), where the relative shift of the slab $\Delta x = 0$, and study the effects of varying slab separation on the optical forces. Since the system has mirror symmetry, the lateral force vanishes. Here we will therefore focus on the behavior of the normal force, as influenced by the dark state discussed in Section 4.1, that occurs at a frequency of $\omega = 0.63 \times 2\pi c / a$ and at $d = d_\infty$.

Figure 3(e) reveals a dark state near $\omega = 0.63 \times 2\pi c / a$ and $d = 0.65a$. Scanning d in the vicinity of d_∞, we plot in Fig. 5 the resonance peak and linewidth, both of which are determined from the transmission spectra. The resonance linewidth indeed vanishes at $d = d_\infty$, consistent with the existence of a dark state at that separation. The linewidth becomes nonzero away as d moves away from d_∞.
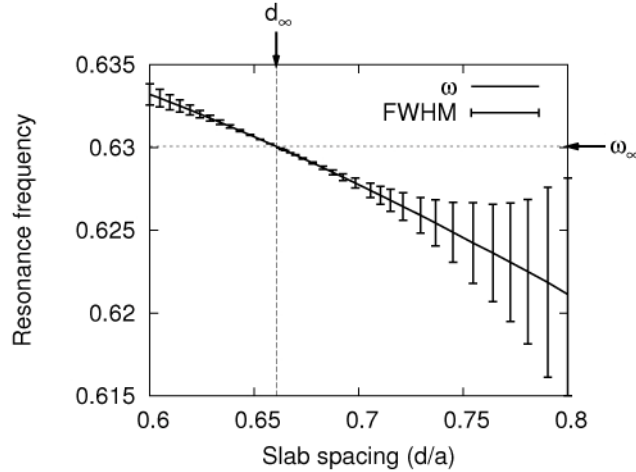

Fig. 5. Resonance peak and linewidth in the vicinity of the dark state arising from coupled bright resonances (Case 1).
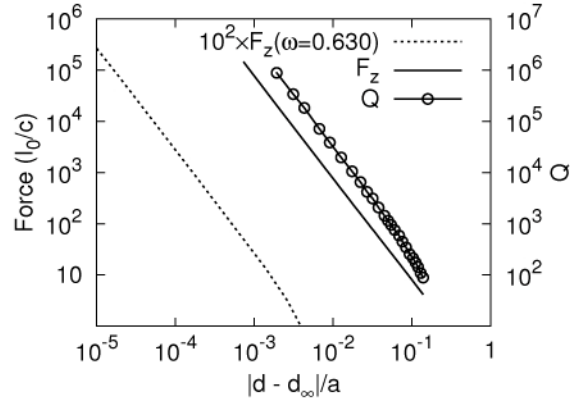

Fig. 6. Divergence behavior of normal force on resonance compared to the *Q* as the slab spacing is varied away from the dark state in Case 1. For reference, the force variation at a constant frequency near the dark state frequency is also plotted with a dashed line.

In Fig. 6 we plot the quality factor of the resonance as a function of *d*. The quality factor was determined by measuring the spectral line width of the resonances. For the resonances of interest, the spectral line shapes are nearly Lorentzian and sufficiently narrowband for this approximation to be accurate. Note that both axes of the plot are on a logarithmic scale and

that the quality factor diverges as $(d - d_\infty)^{-2}$ as d approaches d_∞. Such divergence behavior can be understood as follows: The resonance decay rate, proportional to $1/Q$, must vanish at $d = d_\infty$. Moreover, if one assumes $1/Q$ to be analytic, then the lowest order term must be quadratic since $1/Q$ is non-negative. Hence $1/Q \propto (d - d_\infty)^2$. In Fig. 6, we also plot the force in the direction normal to the slab (F_z) on resonance against slab spacing. The force shows an identical functional dependence (the solid black line in Fig. 6) as the quality factor. Moreover, if we instead consider the force at constant frequency slightly away from the dark state frequency ($\omega = 0.63 \times 2\pi c / a$), the divergence behavior is also identical, as shown in the dotted line. Therefore, in this case the Q enhancement is the dominant mechanism for force enhancement in this system.

It is also interesting to note in Fig. 6, that the same functional dependency persists for values of Q as low as 100. Thus the effects considered here do not require the achievement of extremely high Q factors.
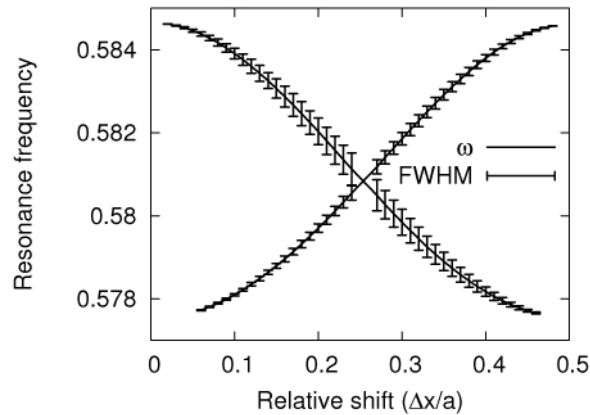

Fig. 7. Resonance peak and linewidth in the vicinity of the dark state arising from coupled dark resonances (Case 2). One of the pair of resonances has a Q much higher than the other, causing its FWHM to appear negligible.

5.2 Case 2: Changing relative shift

We now consider the effect of changing relative shift Δx on the optical forces, as influenced by the dark state in Section 4.2, which occurs near the frequency $\omega = 0.58 \times 2\pi c / a$. In Fig. 7, we plot the resonant properties of the modes as Δx is varied. The resonant linewidth vanishes at $\Delta x = 0$ and $\Delta x = 0.5a$, which correspond the slab configurations that possess mirror symmetry with respect to the yz-plane. Other values of Δx break the mirror symmetry, leading to a non-zero resonant linewidth.

In Fig. 8 the Q of the resonance is plotted as a function of Δx. The Q diverges as Δx^{-2}, which is the lowest order dependence consistent with the requirement that $1/Q$ be a non-negative and analytic function of Δx. Also plotted in Fig. 8 are the forces in the normal direction (F_z) and the lateral direction (F_x). The normal force diverges in the same way as Q, with a Δx^{-2} dependence. The lateral force, however, diverges as Δx^{-1}, leading to certain parameter range within which $\left| F_x \right| > \left| F_z \right|$.

The difference in behaviors for F_z and F_x can be understood as follows: In general, the overall optical force is a product of the force per photon and the number of photons inside the structure. At a given incident power, the number of photons inside the structure is proportional to the quality factor. Thus, in this case it diverges as Δx^{-2}. For the normal force, as seen from Eq. (9), the force per photon has an extremum at $\Delta x = 0$, thus the overall optical force also diverges as Δx^{-2}. On the other hand, the lateral force per photon vanishes at

$\Delta x = 0$, from the symmetry argument as shown in Eq. (10). Hence the lateral force per photon to the lowest order must be proportional to Δx. As a result, the overall lateral force at a constant input power should diverge as Δx^{-1} instead. As we see in this example, the structure symmetry can strongly influence the behavior of the resonant force enhancement.
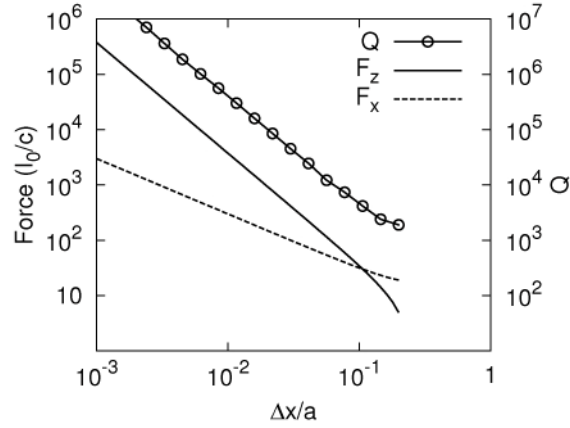

Fig. 8. Divergence behavior of normal and lateral forces on resonance compared to the Q for various shifts near the symmetry point $\Delta x = 0$ for Case 2.
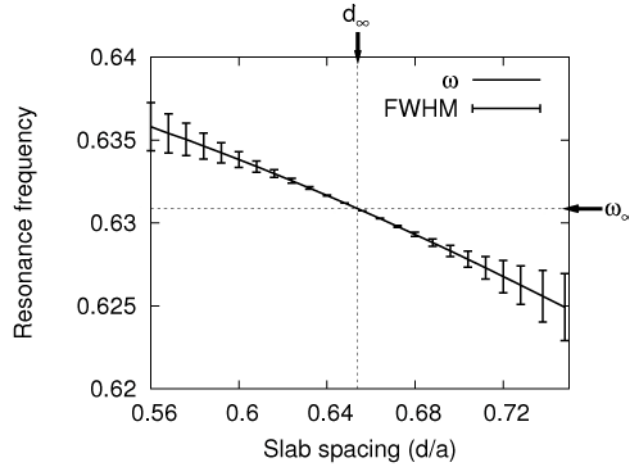

Fig. 9. Resonance peak and linewidth in the vicinity of the dark state for Case 3 at $\Delta x = 0.2a$.

5.3 Case 3: Changing slab separation, asymmetric case

The final case we consider is a system similar to Case 1, except that the two slabs are shifted relative to each other by a distance of $0.2a$, breaking the mirror symmetry with respect to the yz-plane. We again study the behavior of the optical force as a function of slab spacing. In Fig. 9 we plot the resonant properties as a function of slab spacing. We note that with $\Delta x \neq 0$, there still exists a dark state, which in this case occurs at a frequency of $\omega = 0.631 \times 2\pi c / a$ and a slab spacing $d_\infty = 0.65a$. In Fig. 10, we plot the Q, as well as the normal force F_z and the lateral force F_x on resonance, against the slab spacing. They all vary as $(d - d_\infty)^{-2}$, hence the behavior of both the normal and the lateral forces is dominated by the Q enhancement, unlike the Case 2 above. The divergence behavior of the lateral force therefore depends on the symmetry of the structure when it supports a state that is completely dark.
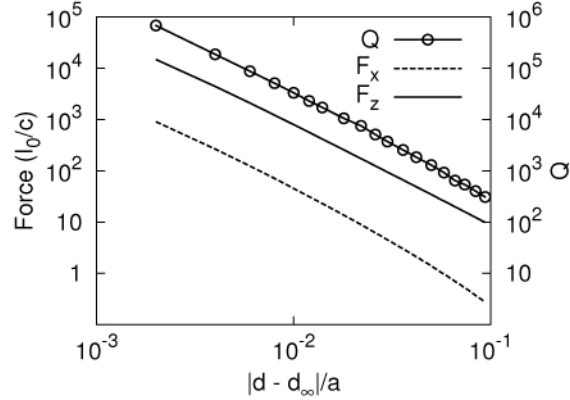
Fig. 10. Divergence behavior of normal and lateral forces on resonance compared to the Q for various slab spacings near the dark state corresponding to $\omega = 0.583 \times 2\pi c / a$ and $\Delta x = 0.2a$ in Fig. 9.

6. Practical realization

Practical realizations of this system may prove to be interesting for optomechanical control, since the magnitude of force obtainable scales roughly with the quality factor of the slab system. The system does not require an extremely high Q in order to observe forces due to the delocalized nature of the fields. The two-slab system is suited for low power excitation since the field is confined in the vertical direction for a distance smaller than the wavelength of light, giving rise to a large enhancement in the near field. For an incident power of 1 mW at 1.5 μm focused on a spot of about 100 μm^2 (an area of approximately $250a^2$) would produce a force of 330 pN assuming a resonator Q of 10^5, a force significantly larger than Van der Waals forces for typical slab separations on the order of the wavelength.

7. Conclusion

We have shown that in the coupled slab system, the optical forces are strongly influenced by the symmetry of the system as well as its resonance properties. The periodic nature of the forces leads to stable and unstable equilibrium configurations of the system. These effects should also generalize to 2D periodic slabs. Under selective excitation of the guided resonances of such slabs, step-like motion and self-trapping can arise [26]. These behaviors may, for example, be useful for automatic alignment of nanostructures.

We have also shown that different types of dark states within a coupled photonic crystal slab system exhibit qualitatively different force divergence behaviors. Generally, the force enhancement scales with the Q of the resonances in the structure even for moderate values of Q. By placing the system configuration in the vicinity of a dark state, a dramatic enhancement of the optical forces may be obtained due to the large resonant enhancement of the fields. Moreover, the enhancement behavior is closely related to some of the symmetry properties of the system. The results presented are applicable for normal incidence. We do, however, expect similarly dramatic lateral force enhancement to arise for non-normal incidence and other polarizations.

Acknowledgments